Magnetic barrier on strained graphene: A possible valley filter

Feng Zhai and Xiaofang Zhao
School of Physics and Optoelectronic Technology and College of Advanced Science and Technology, Dalian University of Technology, Dalian 116024, China

Kai Chang
SKLSM, Institute of Semiconductors, Chinese Academy of Sciences, P.O. Box 912, Beijing 100083, China

H. Q. Xu
Division of Solid State Physics, Lund University, P.O. Box 118, S-22100 Lund, Sweden
(Received 30 March 2010; published 23 September 2010)

We put forward a two-terminal valley filter based on a bulk graphene sheet under the modulations of both a local perpendicular magnetic field and a substrate strain. When only one of the two modulations is present, no valley polarization can be generated. A combination of the two modulations leads to a different (but not opposite) shifts of the K and K' valleys, which could be utilized to generate a valley-polarized current. The degree of the valley polarization can be tuned by the strain strength and the inclusion of a scalar potential. The valley polarization changes its polarity as the local magnetic field switches its direction.

DOI: 10.1103/PhysRevB.82.115442 PACS number(s): 72.80.Vp, 75.70.Ak, 73.43.Cd, 73.23.Ad

I. INTRODUCTION

The peculiar band structure renders graphene a rapidly rising star of low-dimensional materials since its experimental discovery in 2004.[1,2] As a flat layer of carbon atoms arranged in a honeycomb lattice, a graphene material, if in neutrality, has a Fermi surface consisting of two degenerate and inequivalent valleys (K and K') at the corner of the Brillouin zone. The two valleys are related by the time-reversal symmetry. Near each valley point, the bands extend linearly, allowing a massless Dirac-spinor description for elementary excitations in bulk graphene. Such a band character gives rise to many remarkable features of both graphene itself and graphene-based nanostructures, which could be exploited to create novel nanoelectronic and spintronic devices.

Among those features of graphene is Klein tunneling, which leads to the absence of backscattering and thus limits the on-off ratios of graphene-based transistors. An approach to circumvent the Klein tunneling aims at modulating the transverse motion of Dirac electrons. This can be realized, for examples, by means of inhomogeneous magnetic fields[3–5] and substrate strains.[6] Local magnetic fields can be created by depositing nanomagnetic elements on top of graphene films as the way in semiconductor heterostructures.[7,8] The effect of strains on the band structures and optical phonons in graphene samples has been examined experimentally by Raman spectroscopy.[9–11] It has been demonstrated theoretically that the uniaxial strains up to 15% make no significant changes on the graphene band structure.[12]

As a counterpart of electronic spin in spintronics, the valley degree of freedom in graphene has been suggested as information carrier.[13] The operation of valley-based electronic devices requires the generation of an uneven valley distribution of electrons. Intervalley coupling is suppressed in a clean bulk graphene sample. Several schemes for valley filters have been proposed, which concern confined systems[13,14] formed between two zigzag graphene nanoribbons, staggered sublattice potentials,[15] and the trigonal warping effect of graphene bands far away from the Dirac points.[16,17] All of these proposals focus on an all-electrical control of valley polarization. In this work, we put forward a tunable valley filter based on *bulk* graphene under the modulations of both the substrate strains and magnetic fields.

II. MODEL AND FORMALISM

We begin with the comparison between spintronics[18] and valleytronics. It is well known that electronic spin can manifest itself through the coupling to an external magnetic field, especially in semiconductors with a large g factor. In contrast, the intervalley scattering in graphene is negligible even for magnetic fields up to 10^4 T. The spin-orbit interaction (SOI) provides a way to manipulating the spin states of charge carriers by their orbital motion. Due to the time-reversal symmetry, the SOI alone cannot generate a spin polarization in two-terminal waveguide systems when the outgoing lead supports only one orbital mode.[19] In valleytronics, the in-plane strain plays a similar role as the SOI in spintronics. The strain-induced pseudomagnetic field in graphene has opposite signs for the K and K' valleys. As we will show, the elastic deformation alone cannot produce a valley polarization in two-terminal graphene devices. When a magnetic barrier is applied to a strained graphene film, the shifts of the K and K' valleys are neither identical nor opposite, which can be utilized to construct a valley filter.

As shown in Ref. 2, a mechanical in-plane strain in graphene can be described by a gauge vector potential $\mathbf{A}_S(\mathbf{r})$. The projection of $\mathbf{A}_S(\mathbf{r})$ along the zigzag (armchair) direction of the graphene lattice, denoted as A_{SZ} (A_{SA}), can be expressed as

$$A_{SZ} + iA_{SA} = \sum_{\mathbf{n}} \delta t(\mathbf{r},\mathbf{n}) \exp(-i\mathbf{K}\cdot\mathbf{n})$$

$$= c[(u'_{ZZ} - u'_{AA}) + (-2u'_{AZ})i]. \quad (1)$$

Here $\delta t(\mathbf{r},\mathbf{n})$ is the strain-induced changes (at the position $\mathbf{r}$) in the hopping amplitude t along a given nearest-neighbor

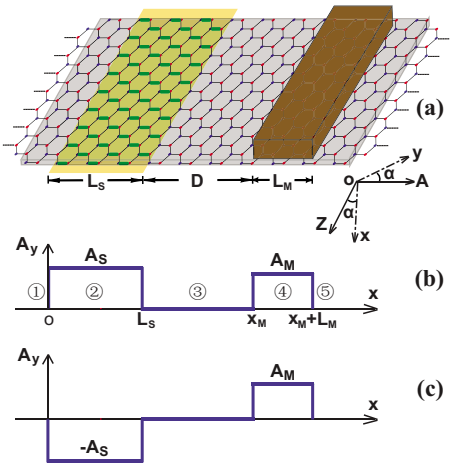

FIG. 1. (Color online) (a) Schematic illustration of the considered graphene device with a dielectric layer and a substrate strain (the left yellow shaded region with thicker bonds). A FM stripe is deposited on the dielectric layer to provide a local magnetic modulation for electrons in the graphene plane. The substrate strain is induced by a tension along the x axis which has an angle α with the zigzag direction of the graphene lattice. In the calculations we take $\alpha=\pi/2$. (b) and (c) Profiles of the total vector potential $A_y(x)$ for electrons in the K and K′ valleys.

vector $\mathbf{n}$, $\mathbf{K}$ is the wave vector of the Dirac point K, $c>0$ is a constant, and u'_{ZZ}, u'_{AA}, and u'_{AZ} are the components of the strain tensor in the lattice coordinate system ZoA. The amplitude of the strain can be estimated as $|\delta t|/t$ with $t \approx 3$ eV. The strain considered in our work is assumed to be homogeneous in a given direction which is taken as the y axis, i.e., $u_{ij}(\mathbf{r})=u_{ij}(x,y=0)$ with $i,j \in \{x,y\}$. The y axis may deviate from the armchair direction with an angle α [see Fig. 1(a)]. Such a strain distribution can be induced by a uniform tension along the x direction, applied on the substrate rather than the graphene (which adheres to the top of the substrate).[9] We rotate the strain tensor u_{ij} through an angle $-\alpha$ to obtain A_{SZ} and A_{SA}. The components of $\mathbf{A}_S$ in the xoy coordinate system are then given by

$$\begin{pmatrix} A_{Sx} \\ A_{Sy} \end{pmatrix} = c \begin{pmatrix} \cos 3\alpha & \sin 3\alpha \\ -\sin 3\alpha & \cos 3\alpha \end{pmatrix} \begin{pmatrix} u_{xx}-u_{yy} \\ -2u_{xy} \end{pmatrix}. \quad (2)$$

This expression respects the symmetry of the graphene lattice.

The inclusion of a magnetic barrier introduces a magnetic vector potential $\mathbf{A}_M(\mathbf{r})$. We assume that the magnetic barrier is created by a ferromagnetic metal (FM) stripe, which is in parallel with the y direction and has a magnetization along the x axis, placing on the top of the graphene film [see Fig. 1(a)]. The magnetic vector potential in the Landau gauge is thus of the form $\mathbf{A}_M(\mathbf{r})=A_M(x)\mathbf{e}_y$. When a scalar potential $U(\mathbf{r})=U(x)$ is further considered, the low-energy Hamiltonian for electrons in a given valley reads

$$H_\xi = v_F \sigma \cdot (\mathbf{p} + e\mathbf{A}_M + \xi \mathbf{A}_S/v_F) + U\sigma_0, \quad (3)$$

where $v_F \approx 0.86\times 10^6$ m/s is the Fermi velocity, $\mathbf{p}=(p_x,p_y)$ is the in-plane momentum of electrons in graphene, σ_x and σ_y are Pauli matrices, $\xi=\pm 1$ for the K and K' valleys, and σ_0 is the 2×2 unit matrix. Note that in our formulation the x component of $\mathbf{A}_S$ can be removed by a local unitary transformation $u(x)=\exp[-i\xi\int_{-\infty}^{x} A_{Sx}(x')dx'/(\hbar v_F)]$. The value of A_{Sy} depends both on the strain u_{ij} and the angle α.

Since the system is invariant translationally along the y direction, the transverse wave vector k_y is conserved. We use $t_\xi(E,k_y)$ to denote the transmission amplitude of electrons incoming from the ξ valley with energy E. For a general profile of the vector potential $\mathbf{A}_M(x)$, $\mathbf{A}_S(x)$ and the scalar potential $U(x)$, the transmission amplitude can be calculated numerically by means of the scattering matrix method.[20] At a low temperature T_K, the valley-resolved conductance is given by

$$G_\xi(E_F) = \frac{2e^2}{h} \int dE \frac{-\partial f}{\partial E} \int_{-|E|/\hbar v_F}^{+|E|/\hbar v_F} |t_\xi(E,k_y)|^2 \frac{dk_y}{2\pi/L_y}, \quad (4)$$

where E_F is the Fermi energy, L_y is the sample size along the y direction, and $f(E)=\{1+\exp[(E-E_F)/(k_BT_K)]\}^{-1}$ is the Fermi-Dirac distribution function. The valley polarization is defined as

$$P = \frac{G_{+1}-G_{-1}}{G_{+1}+G_{-1}}. \quad (5)$$

The operation $S=i\sigma_y C$ (C is the operator of complex conjugation) transforms the Hamiltonian $H_\xi(\mathbf{A}_M)$ to $H_{-\xi}(-\mathbf{A}_M)$. Such an observation results in[19]

$$|t_{-\xi}(E,k_y;\mathbf{A}_M)|^2 = |t_\xi(E,-k_y;-\mathbf{A}_M)|^2. \quad (6)$$

The combination of Eqs. (4)–(6) yields that the polarity of the valley polarization is reversed ($P\to -P$) as the magnetic barrier switches its direction ($\mathbf{A}_M \to -\mathbf{A}_M$). Particularly, in the absence of the magnetic barrier ($\mathbf{A}_M=0$), the valley polarization vanishes, which indicates that the strain alone cannot generate a valley-polarized current in a two-terminal graphene device. The inclusion of a magnetic barrier breaks the symmetric relation between H_{+1} and H_{-1}, allowing a valley dependence of the conductance. Obviously, when the strain-induced vector potential $\mathbf{A}_S$ changes to $-\mathbf{A}_S$, the valley polarization is also reversed.

In order to demonstrate the operating principle of the device, we set $\alpha=\pi/2$ and take a simplified gauge field $\mathbf{A}_S(\mathbf{r})$ as in Ref. 6,

$$\mathbf{A}_S(\mathbf{r}) = A_S\Theta(x)\Theta(L_S-x)\mathbf{e}_y, \quad (7)$$

which accounts for a uniform perturbation $\delta t \equiv A_S$ of the hopping along the x direction, over a region $x\in[0,L_S]$. The magnetic barrier is approximated to be of a double-spikelike shape, for which the magnetic vector potential has the form

$$\mathbf{A}_M = A_M\Theta(x-x_M)\Theta(L_M+x_M-x)\mathbf{e}_y. \quad (8)$$

Here A_M and L_M represent the strength and width of the magnetic barrier, $x_M=L_S+D$ with D the distance between the magnetic barrier and the strain region. The scalar potential U is U_S (U_M) in the strain (magnetic barrier) region and zero otherwise. Note that U_M can be tuned by the voltage applied on the FM stripe. For convenience we use the units with a length scale $l_{B_0}=\sqrt{\hbar/eB_0}$ and energy scale $E_0=\hbar v_F/l_{B_0}$, which are 811 Å and 7.0 meV, respectively, for a typical

magnetic field $B_0=0.1$ T. For example, the conductance unit is taken as $G_0=e^2(L_y/l_{B_0})/(\pi h)$ and the temperature is in unit of E_0/k_B. The distributions of the total (dimensionless) vector potential $A_y(x)=A_M(x)+A_S(x)$ for the two valleys are shown in Figs. 1(b) and 1(c).

For the simplified pontetial profile, the transmission can be derived analytically. In a given region j [denoted in Fig. 1(b)], the vector potential $A_y=A_{yj}$ and the scalar potential $U=U_j$ are constant, which enables us to introduce a longitudinal wave vector of electrons with incident energy E and wave vector k_y,

$$k_{xj}=\mathrm{sgn}(E_j)\sqrt{E_j^2-k_{yj}^2}, \tag{9}$$

where $E_j=E-U_j$, and $k_{yj}=k_y+A_{yj}$. Note that $k_{x1}=k_{x3}=k_{x5}$ while k_{x2} is valley dependent. For the considered electron transporting through the magnetic barrier region from the left, the transmission and reflection amplitudes are given by

$$t_M=\frac{k_{x1}k_{x4}}{k_{x1}k_{x4}\cos\phi+i(k_{y1}k_{y4}-E_1E_4)\sin\phi}, \tag{10}$$

$$r_M=\frac{E_1^{-1}(k_{x1}+ik_{y1})(k_{y1}E_4-k_{y4}E_1)\sin\phi}{k_{x1}k_{x4}\cos\phi+i(k_{y1}k_{y4}-E_1E_4)\sin\phi}, \tag{11}$$

where $\phi=k_{x4}L_M$. For the incidence from the right, the reflection amplitude becomes

$$r'_M=\frac{E_1^{-1}(-k_{x1}+ik_{y1})(k_{y1}E_4-k_{y4}E_1)\sin\phi}{k_{x1}k_{x4}\cos\phi+i(k_{y1}k_{y4}-E_1E_4)\sin\phi}. \tag{12}$$

Note that $|t_M|^2$, $|r_M|^2$, and $|r'_M|^2$ are invariant under the substitution of both $k_{y1}\to-k_{y1}$ and $k_{y4}\to-k_{y4}$. The scattering amplitudes for the same electron traversing the strain region, denoted as $t_{S;\xi}$, $r_{S;\xi}$, and $r'_{S;\xi}$, can be calculated from Eqs. (10)–(12) with the replacement $k_{x4}\to k_{x2}$, $k_{y4}\to k_{y2}$, $E_4\to E_2$, and $\phi\to k_{x2}L_S$. Because the considered problem is equivalent to a double-barrier tunneling, the transmission amplitude reads

$$t_\xi=\frac{t_{S;\xi}t_M\exp(ik_{x1}D)}{1-r'_{S;\xi}r_M\exp(2ik_{x1}D)}. \tag{13}$$

For the transmission determined by Eqs. (10)–(13), the general result Eq. (6) can be verified.

III. NUMERICAL RESULTS AND DISCUSSIONS

In Fig. 2, we present the valley-dependent transmission $|t_\xi|^2$ as a function of the incident angle θ and electron energy E. To reduce the number of adjustable parameters, here and hereafter we take the structural parameters as $L_M=L_S=D=1$ and set $A_M=2$ and $U_M=U_S$ without specification. The appearance of the direction-dependent transmission blockade and resonant tunneling can be explained from the condition for the existence of evanescent modes in the magnetic barrier or strain region.[5,6] Since such a condition depends strongly on the global profile of A_y, a large difference in the transmission spectrum is expected for the K and K' electrons. Actually, one can observe from Fig. 2 that under a suitable incident energy E, the K electrons can transmit through the system in a broad region of the incident angle θ while the K' electrons are almost totally reflected in the whole region of θ. The transmission can be further tuned by the strain strength. For the case that A_M (A_S) is much larger than A_S (A_M), the angular anisotropy is caused mainly by the magnetic barrier (strain), as reflected from the transmission features of $E<0$. Under the given parameters, the case $A_S=A_M$ gives rise to the strongest contrast for the transmission of K and K' electrons with a positive energy.

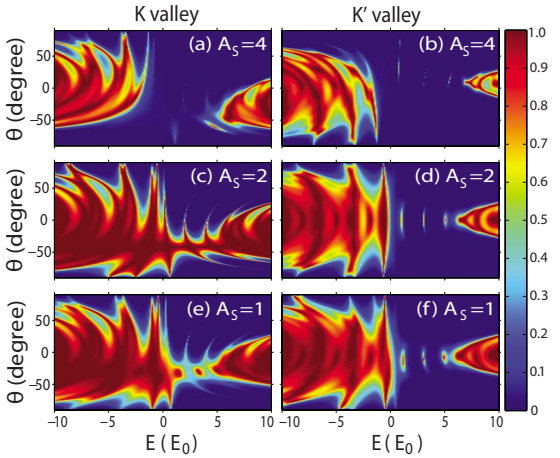

FIG. 2. (Color online) Contour plot of valley-dependent transmission $|t_\xi|^2$ for the K and K' electrons (left and right panels, respectively) traversing the valley filter in Fig. 1(a). We set $U_S=3$ and take A_S as 4 in top panels, 2 in middle panels, and 1 in bottom panels.

The transmission difference between the K and K' electrons can be reflected in the conductance. Figure 3 shows the valley-dependent conductance and the corresponding valley polarization. The zero-temperature conductance (not shown here) exhibits a rich oscillation feature as a consequence of the transmission resonances. At a relative high temperature $T_K=0.5$, the oscillations are washed out. The conductance for

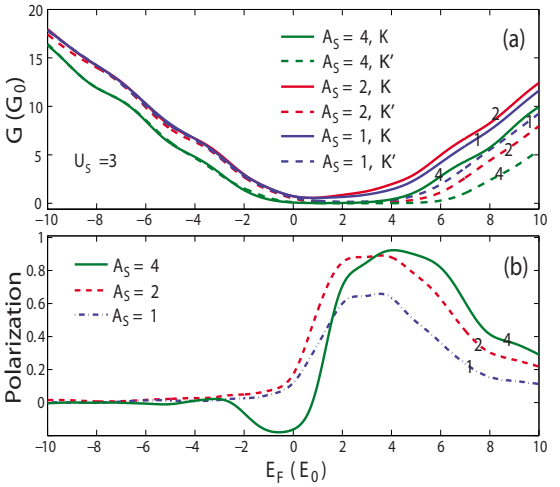

FIG. 3. (Color online) (a) Valley-dependent conductance and (b) valley polarization for the valley filter in Fig. 1(a) plotted as a function of the Fermi energy E_F at a given temperature $T_K=0.5$. We set $U_S=3$. The value of A_S is marked in each curve.

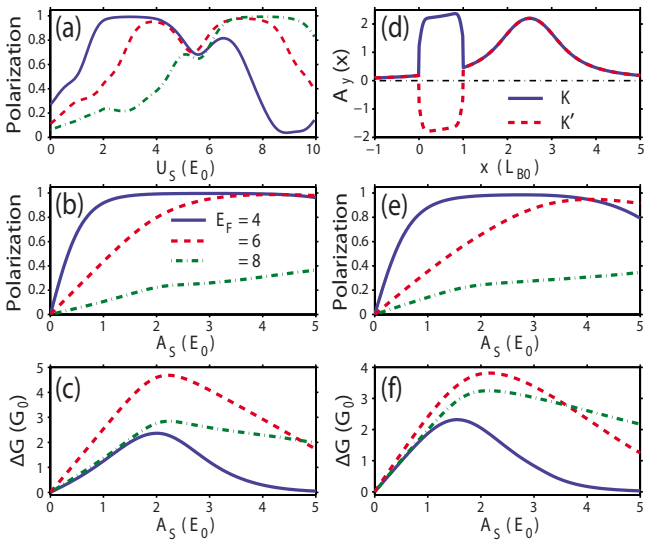

FIG. 4. (Color online) Valley polarization P and conductance difference ΔG for the valley filter in Fig. 1(a) plotted as a function of either U_S or A_S. (a)–(c) results for the simplified profiles of the vector potential in Figs. 1(b) and 1(c). (d) A smooth distribution of the vector potential for $A_S=2$ (see text). (e) and (f) results for a realistic magnetic field profile and a smooth shape of $A_S(x)$. In (a) we set $A_S=2$. In (b), (c), (e), and (f) we take $U_S=3$. The temperature is $T_K=0.1$. In all of the calculations, three values of the Fermi energy are considered: $E_F=4$, 6, and 8.

$E_F<0$ is determined dominantly by $\max(A_S,A_M)$ and has a weak valley dependence. We thus focus only on the case $E_F>0$. It can be seen that for $E_F>U_S$, the conductance of the K electrons is usually larger than that of the K' electrons. This can be understood from the shifts of the Dirac point in the magnetic barrier and the strain region, $\delta\mathbf{k}_M$ and $\delta\mathbf{k}_S$, which are in the same (opposite) direction for the K (K') valley [see Figs. 1(b) and 1(c)]. In comparison with the antiparallel case of $\delta\mathbf{k}_M$ and $\delta\mathbf{k}_S$, there are more available open transmission channels for the parallel shifts. The conductance G_ξ is suppressed when the transmission channel is depleted by the vector potential. Note that in a broad energy region, G_{+1} is finite while G_{-1} is rather small. This interesting feature enables the generation of a valley-polarized injection currents since the system filters out the K component of the electron current. One can achieve a valley polarization exceeding 80% together with a remarkable total conductance [Fig. 3(b)]. Similar to the spin current, the valley current in the linear-response regime is characterized by $\Delta G=G_{+1}-G_{-1}$. Note that in the high Fermi-energy region ΔG varies slowly with E_F while P decreases monotonically.

A tunable valley-polarized source is desirable for valleytronic applications. The tunability of valley filtering for the device shown in Fig. 1(a) is demonstrated in Figs. 4(a)–4(c). The valley polarization can be tuned by both the scalar potential U_S and the strain-induced vector potential A_S. For a given Fermi energy as in Fig. 4(a), the valley polarization is nearly perfect in a wide region of U_S. The reason is that the number of open channels responsible for the conductance G_ξ depends on U_S. For a fixed U_S and E_F, the valley polarization shows a rapid increase with A_S when $|U_S-E_F|$ is small [see Fig. 4(b)]. The difference between the two valley conductances (ΔG) vanishes for the two limiting cases: $A_S \ll A_M$ and $A_S \gg A_M$ [see Fig. 4(c)], as expected from the symmetry analysis. The maximum of ΔG and the A_S position of the maximum depend on both U_S and E_F.

All results presented so far are calculated for a simplified profile of the magnetic barrier. In realistic cases, the modulated magnetic field varies smoothly on the scale of the graphene lattice constant. For definiteness, we assume that the FM stripe in Fig. 1(a) has a magnetization $\mu_0 M=1.8$ T (achievable for Co or Dy material[8]), a rectangular cross section of width $L_M=1$ and height $h=0.6$, and is placed at a distance $z_0=0.2$ to the graphene plane. In this case the generated fringe field can be obtained analytically.[21] Furthermore, we take a smooth profile for the strain-induced gauge potential: $A_{Sy}(x)=A_S\{\Theta(x)\mathrm{erf}(x/b)+\Theta(L_S-x)\mathrm{erf}[(L_S-x)/b]\}/2$. Here $\mathrm{erf}(x)$ is the error function, $b=0.1$ and $L_S=1$. Such a gauge potential corresponds to an effective pseudomagnetic field $B_{eff}=[\xi d A_{Sy}(x)/dx]\mathbf{e}_z$. Note that it is the total variation in $A_{Sy}(x)$ rather than the detail of B_{eff} over the edge smearing region that has a crucial influence on the tunneling suppression.[6] The valley-dependent vector potential $A_y(x)$ for $A_S=2$ is shown in Fig. 4(d). A common feature of the smooth and the simplified A_y distribution is that for the K (K') valley $A_y(x)$ keeps (changes) its polarity from the strain region to the magnetic barrier region. It is this common feature that leads to a similar behavior of valley filtering for both kinds of A_y profiles [see Figs. 4(e) and 4(f)]. The reason is that under this condition the phase-space-related tunneling suppression[6] depends strongly on the valley degree of freedom. This indicates that the detail of the magnetization and strain profile has no drastic effect on the valley polarization characteristics of the valley filter proposed here.

Finally, we would like to give some remarks. Our proposal is based on bulk graphene and the energy spectrum near the Dirac point. Note that most of the excitement about graphene stems from the low-energy regime. Previous proposals on valley filtering require either a precise tailoring of the graphene nanoribbon samples or the band warping effect far away from the Dirac point. The combination of a substrate strain and a local magnetic field provides another path for valley control. Short-range disorder mixing the two valleys will reduce the degree of valley polarization. The intervalley mean-free path is estimated to be of the order 1 μm.[22] Thus the valley polarization considered here should be not degraded substantially when realistic system parameters are considered. The valley-polarized current may be detected by a superconducting contact as in Ref. 23 and can be injected to other valleytronic devices for further manipulation.

IV. CONCLUSIONS

In summary, we have examined the feasibility of generating a valley-polarized current in a two-terminal device based on the bulk graphene material. The proposed valley filter relies on the combination of the two ways utilized to control the transverse motion of Dirac electrons: the local perpendicular magnetic field and the substrate strain. Such a combination shifts the K and K' valleys with different but not

opposite displacements. For the valley polarization, its amplitude can be tuned by the strain strength and the inclusion of a scalar electric potential while its polarity changes as the local magnetic field switches its direction.

ACKNOWLEDGMENTS

This work was supported by NSFC (Grants No. 10704013, No. 60525405, and No. 10874175), RFDP (Grant No. 200801411042), the Fundamental Research Funds for the Central Universities (Grant No. DUT10LK36), and the Swedish International Development Cooperation Agency (SIDA). K. C. acknowledges support from the Chinese Academy of Sciences. H.Q.X. acknowledges support from the Swedish Research Council VR and from the Swedish Foundation for Strategic Research SSF through the Nanometer Structure Consortium at Lund University.

[1] A. K. Geim and K. S. Novoselov, Nature Mater. **6**, 183 (2007).
[2] A. H. Castro Neto, F. Guinea, N. M. R. Peres, K. S. Novoselov, and A. K. Geim, Rev. Mod. Phys. **81**, 109 (2009).
[3] A. De Martino, L. Dell'Anna, and R. Egger, Phys. Rev. Lett. **98**, 066802 (2007).
[4] M. Ramezani Masir, P. Vasilopoulos, A. Matulis, and F. M. Peeters, Phys. Rev. B **77**, 235443 (2008).
[5] F. Zhai and K. Chang, Phys. Rev. B **77**, 113409 (2008).
[6] V. M. Pereira and A. H. Castro Neto, Phys. Rev. Lett. **103**, 046801 (2009).
[7] For a review, see S. J. Lee, S. Souma, G. Ihm, and K. J. Chang, Phys. Rep. **394**, 1 (2004).
[8] For recent work, see, for example, J. Hong, S. Joo, T.-S. Kim, K. Rhie, K. H. Kim, S. U. Kim, B. C. Lee, and K.-H. Shin, Appl. Phys. Lett. **90**, 023510 (2007); M. Cerchez, S. Hugger, T. Heinzel, and N. Schulz, Phys. Rev. B **75**, 035341 (2007); A. Tarasov, S. Hugger, H. Xu, M. Cerchez, T. Heinzel, I. V. Zozoulenko, U. Gasser-Szerer, D. Reuter, and A. D. Wieck, Phys. Rev. Lett. **104**, 186801 (2010).
[9] Z. H. Ni, T. Yu, Y. H. Lu, Y. Y. Wang, Y. P. Feng, and Z. X. Shen, ACS Nano **2**, 2301 (2008); **3**, 483 (2009).
[10] T. M. G. Mohiuddin, A. Lombardo, R. R. Nair, A. Bonetti, G. Savini, R. Jalil, N. Bonini, D. M. Basko, C. Galiotis, N. Marzari, K. S. Novoselov, A. K. Geim, and A. C. Ferrari, Phys. Rev. B **79**, 205433 (2009).
[11] M. Huang, H. Yan, C. Chen, D. Song, T. F. Heinz, and J. Hone, Proc. Natl. Acad. Sci. U.S.A. **106**, 7304 (2009).
[12] V. M. Pereira, A. H. Castro Neto, and N. M. R. Peres, Phys. Rev. B **80**, 045401 (2009); M. Farjam and H. Rafii-Tabar, *ibid.* **80**, 167401 (2009).
[13] A. Rycerz, J. Tworzydło, and C. W. J. Beenakker, Nat. Phys. **3**, 172 (2007).
[14] Z. Z. Zhang, K. Chang, and K. S. Chan, Appl. Phys. Lett. **93**, 062106 (2008).
[15] D. Xiao, W. Yao, and Q. Niu, Phys. Rev. Lett. **99**, 236809 (2007).
[16] J. L. Garcia-Pomar, A. Cortijo, and M. Nieto-Vesperinas, Phys. Rev. Lett. **100**, 236801 (2008).
[17] M. Pereira, Jr., F. M. Peeters, R. N. Costa Filho, and G. A. Farias, J. Phys.: Condens. Matter **21**, 045301 (2009).
[18] I. Žutić, J. Fabian, and S. Das Sarma, Rev. Mod. Phys. **76**, 323 (2004).
[19] F. Zhai and H. Q. Xu, Phys. Rev. Lett. **94**, 246601 (2005).
[20] H. Xu, Phys. Rev. B **50**, 8469 (1994).
[21] I. S. Ibrahim and F. M. Peeters, Phys. Rev. B **52**, 17321 (1995).
[22] F. V. Tikhonenko, D. W. Horsell, R. V. Gorbachev, and A. K. Savchenko, Phys. Rev. Lett. **100**, 056802 (2008).
[23] A. R. Akhmerov and C. W. J. Beenakker, Phys. Rev. Lett. **98**, 157003 (2007).